BÉRAR, J. F. & LELANN, P. (1991). *J. Appl. Cryst.* **24**, 1–5.
BOULTIF, A. & LOUËR, D. (1991). *J. Appl. Cryst.* **24**, 987–993.
BUSSEREAU, I., BELKHIRIA, M. S., GRAVEREAU, P., BOIREAU, A., SOUBEYROUX, J. L., OLAZCUAGA, R. & LE FLEM, G. (1992). *Acta Cryst.* C**48**, 1741–1744.
EL JAZOULI, A., SERGHINI, A., BROCHU, R., DANCE, J. M. & LE FLEM, G. (1985). *C. R. Acad. Sci.* **300**, 493–496.
FAIR, C. K. (1990). *MolEN. An Interactive Intelligent System for Crystal Structure Analysis.* Enraf–Nonius, Delft, The Netherlands.
FARGIN, E., BUSSEREAU, I., OLAZCUAGA, R., LE FLEM, G., CARTIER, C. & DEXPERT, H. (1994). *J. Solid State Chem.* **112**, 176–181.
GALESIC, N., MATKOVIC, B., TOPIC, M., COFFOU, E. & SLJUKIC, M. (1984). *Croat. Chem. Acta*, **57**(4), 597–608.
ISHIGURO, L., KITAZAWA, A., MITUZANI, N. & KATO, M. (1981). *J. Solid State Chem.* **40**, 170–174.
KEESTER, K. L. & JACOBS, J. T. (1974). *Ferroelectrics*, **8**, 657–664.
LAÜGT, M. (1973). *J. Appl. Cryst.* **6**, 299–301.
LE POLLES, G., EL JAZOULI, A., OLAZCUAGA, R., DANCE, J. M., LE FLEM, G. & HAGENMULLER, P. (1987). *Mater. Res. Bull.* **22**, 1171–1177.
LE POLLES, G., PARENT, C., OLAZCUAGA, R., LE FLEM, G. & HAGENMULLER, P. (1988). *C. R. Acad. Sci.* **306**, 765–768.
LOUËR, D. & LANGFORD, J. I. (1988). *J. Appl. Cryst.* **21**, 430–437.
MATKOVIC, B., PRODIC, B. & SLJUKIC, M. (1968). *Bull. Soc. Chim. Fr.* 1777–1779.
MATKOVIC, B., PRODIC, B., SLJUKIC, M. & PETERSON, S.W. (1968). *Croat. Chem. Acta*, **40**, 147–160.
MATKOVIC, B., PRODIC, B., SLJUKIC, M., TOPIC, M., WILLET, R. D. & PULLEN, F. (1970). *Inorg. Chim. Acta*, **4**, 571–576.
MARINDER, B. O. & WAHLSTRÖM, E. (1984). *Chem. Scr.* **23**, 157–160.
MBANDZA, A., BORDES, E. & COURTINE, P. (1987). *Mat. Res. Bull.* **20**, 251–257.
MCCARRON, E. M., CALABRESE, J. C. & SUBRAMANIAN, M. B. (1987). *Mater. Res. Bull.* **22**, 1421–1426.
RODRIGUEZ-CARVAJAL, J. (1990). Collected Abstracts of Powder Diffraction Meeting, Toulouse, France, July 1990, p. 127.
SCHMID, W. F. & MOONEY, R. W. (1964). *J. Electrochem. Soc.* **111**, 668–673.
SERGHINI, A. (1984). Thesis, University of Rabat (Morocco).
SERGHINI, A., BROCHU, R., GRAVEREAU, P. & OLAZCUAGA. R. (1995). To be published.
SERGHINI, A., KACIMI, M., ZIYAD, M. & BROCHU, R. (1988). *J. Chim. Phys. Chim. Biol.* **85**(4), 449–504.
SWANSON, H. E. & FUYAT, R. K. (1953). *Natl. Bur. Stand. (US) Circ.* **539**, 23–25.
YAO, P. C. & FRAY, D. J. (1983). *Solid State Ion.* **8**, 35–42.

Acta Cryst. (1995). B**51**, 913–920

Electron Density – Structure Relationships in Some Perovskite-Type Compounds

BY J. R. HESTER* AND E. N. MASLEN

Crystallography Centre, University of Western Australia, Nedlands 6907, *Australia*

(*Received* 20 *June* 1994; *accepted* 8 *March* 1995)

Abstract

Experimentally measured electron-deformation densities for the structurally related compounds dipotassium palladium tetrachloride, K_2PdCl_4, dipotassium silicon hexafluoride, K_2SiF_6, dipotassium palladium hexachloride, K_2PdCl_6, and dipotassium nickel tetrafluoride, K_2NiF_4, contain significant features in interatomic regions. The topographical relationship of interatom depletions to the structural geometry indicates that they originate from non-bonded interactions between atoms. The $\Delta\rho$ maps for K_2PdCl_4 and K_2PdCl_6 show unexpected structure near the K atoms. Low-temperature studies on K_2SiF_6 and K_2PdCl_4 indicate that these features are not due to anharmonic thermal motion, in marked contrast to those near the halide atoms. For the new low-temperature analysis included in the study: K_2SiF_6, cubic, $Fm\bar{3}m$, $M_r = 220.27$, $a = 8.046\,(2)$ Å, $V = 520.9\,(4)$ Å^3, $Z = 4$, $D_x = 2.81\,(2)$ Mg m^{-3}, μ(Mo $K\alpha$) = 2.09 mm^{-1}, $F(000) = 424$, $T = 110$ K, $R = 0.070$, $wR = 0.024$, $S = 1.47\,(9)$ for 129 independent reflections.

Introduction

Most accurate diffraction imaging studies focus on bonding-related deformation of the electron density near the shorter interatom vectors linking atomic nuclei. Several previous studies of simple inorganic compounds have reported significant accumulation and depletion in regions further from the nuclei. Electron-difference-density features persist in these regions even when the structure refinement model includes local multipole expansions of the electron density.

Maslen & Spadaccini (1989) identified consistent trends at structural cavities in measured $\Delta\rho$ maps for a series of transition-metal perovskite compounds. Their findings were confirmed and amplified in studies of $KCuF_3$ by Buttner, Maslen & Spadaccini (1990), and of $KZnF_3$ by Maslen, Spadaccini, Ito, Marumo, Tanaka & Satow (1993), who also identified $\Delta\rho$ depletions around the structural cavities.

Such evidence is frequently ignored or attributed to random experimental error and/or accumulation of systematic error near special positions. The possibility that these features are related to random errors can be investigated by replicating experiments. Accumulation of error at special positions cannot explain extended interatomic

* Present address: National Institute for Research in Inorganic Materials, Namiki 1-1, Tsukuba, Ibaraki 305, Japan.

Table 1. *Selected experimental and refinement details*

	K_2SiF_6[a]	K_2SiF_6 (low temperature)[b]	K_2PdCl_6[a]	K_2PdCl_4[c]	K_2PdCl_4[d] (low temperature)	K_2NiF_4[e]
Space group	$Fm\bar{3}m$,	$Fm\bar{3}m$,	$Fm\bar{3}m$,	$P4/mmm$	$P4/mmm$	$I4/mmm$
Radiation	Synchrotron	Tube	Synchrotron	Synchrotron	Tube	Tube
Wavelength (Å)	0.9	Mo $K\alpha$	0.9	0.9	Mo $K\alpha$	Mo $K\alpha$
Temperature	Room	110 K	Room	Room	120 K	Room
Max. $\sin\theta/\lambda$	1.00	0.95	1.01	1.01	1.22	1.36
$\sigma(\Delta\rho)$	0.04	0.21	0.04	0.03	1.14	0.08
Extinction refined	No	No	Yes	No	Yes	Yes

References: (*a*) Hester *et al.* (1993*a*); (*b*) reported here; (*c*) Hester *et al.* (1993*b*); (*d*) Takazawa *et al.* (1988*a*), (*e*) Yeh *et al.* (1993*a*).

features. Such accumulation diminishes sharply with distance from the symmetry element.

Electron densities measured accurately for structures related to simple perovskites have not yet been synthesized in earlier studies. Six experiments are compared below, paying special attention to the difference density in interatomic regions, especially near K atoms that would not normally be associated with strongly directed bonding. Full details of the original experiments are given in the papers by Hester, Maslen, Spadaccini, Ishizawa & Satow (1993*a*,*b*), Yeh, Wu, Lee & Wang (1993) and Takazawa, Ohba & Saito (1988). The relevant information is summarized in Table 1. An original low-temperature experiment that is germane to the comparison is also described in these papers.

The three structures involved share common characteristics. Each is composed of three types of atoms. All contain coordinating halide atoms and ionically bonded K atoms. Two structures (K_2SiF_6/K_2PdCl_6 and K_2NiF_4) contain one sixfold and one (K_2PdCl_4) fourfold coordinated metal. For convenience, Si is referred to as a metal throughout this paper. In those structures where the metal is coordinated octahedrally, the K atoms are located along the <111> directions of the octahedron. The K atoms in K_2PdCl_4 are at analogous positions, such that the Pd–K vector, which lies in a plane containing the bisector of the angle formed by neighbouring Pd—Cl bonds and the normal to the $PdCl_4$ moiety, makes a 30° angle with the bond plane. In K_2NiF_4 the Ni atom shares four F atoms with neighbouring NiF_6 moieties.

The halide environment consists of (i) the metal atom to which the halide atom X is bonded, (ii) other ligating halide atoms and (iii) K atoms. In K_2SiF_6 and K_2PdCl_6 the K and X atoms are virtually coplanar. There is an M–X vector perpendicular to this plane and a similarly oriented X–X vector linking neighbouring MX_6 moieties across a structural cavity. In K_2PdCl_4, Cl atoms also face each other across a structural cavity in the $z = 0$ plane. In K_2NiF_4 there are two symmetrically distinct halide atoms. F1 is bonded symmetrically to two Ni atoms. On the other hand, the F2 atom in K_2NiF_4 is collinear with Ni and K atoms, forming planes with K atoms similar to those in K_2SiF_6.

The particularly simple K, Ni and F atom configuration of the ideal cubic perovskite structure that occurs in $KNiF_3$ at room temperature (Kijima, Tanaka & Marumo, 1983) is virtually identical to that near the base plane for K_2NiF_4, which has four NiF_6 moieties as with K atoms at $\frac{1}{2}, \frac{1}{2}, 0.15$. The a-cell dimensions reflect this similarity. In $KNiF_3$ $a = 4.0115\,(7)$ Å, compared with $a = 4.0130\,(6)$ Å in K_2NiF_4 (Yeh *et al.*, 1993).

The common structural motifs described above should be reflected in similarities between the electron densities for these compounds. The degree of correspondence between deformation densities in the regions where the K_2NiF_4 and $KNiF_3$ structures correspond thus provides a further check on the reliability of measured $\Delta\rho$ maps.

The paper first describes two previously unpublished low-temperature experiments. Before comparing the experimentally measured electron densities, their reliability is assessed. Significant peaks and depressions in experimental $\Delta\rho$ for the structures described above are listed and their origin is elucidated. The final section deals explicitly with $\Delta\rho$ features near K atoms.

Low-temperature experiments

An accurate low-temperature study of K_2PdCl_4 was reported by Takazawa *et al.* (1988). Because achieving consistency in low-temperature diffraction imaging is difficult, a new experiment was undertaken to confirm the reliability of the earlier study. The two experiments agree closely, especially after modifying the Takazawa *et al.* (1988) procedure slightly by treating weights identically in both refinements. The $\Delta\rho$ maps described in Fig. 4(*b*) were evaluated using the higher-resolution data deposited by Takazawa *et al.* (1988). Experimental details and refined parameters for the new determination have been deposited.*

No previous accurate low-temperature electron density experiment for K_2SiF_6 has been reported. A crystal with morphology and dimensions similar to that for the synchrotron room-temperature study of Hester *et al.* (1993*a*) was glued to a thin glass fibre

* Lists of structure factors and isotropic and atomic displacement parameters have been deposited with the IUCr (Reference: AS0671). Copies may be obtained through The Managing Editor, International Union of Crystallography, 5 Abbey Square, Chester CH1 2HU, England.

and mounted in a steady stream of boil-off nitrogen on a $P2_1$ diffractometer. A temperature of 110 (10) K was maintained by monitoring thermocouple measurements at the exit nozzle, adjusting the current through a small heater in the gas stream automatically.

Two complete spheres of data were measured at a constant scan rate of 12° min^{-1}. The high scan rate minimized condensation of ice that tended to form if the goniometer head was stationary for long periods. Experimental details are listed in Table 2.

All 002 reflections and equivalents, measured twice for a total of 12 measurements, had atypical profiles that were either flat or sloped upwards in a positive $\omega/2\theta$ direction. The weak reflections with strongly sloping profiles had unusually imbalanced backgrounds, leading in several cases to net negative intensities. These uneven backgrounds appear to be connected to strong, asymmetric diffuse scattering, perhaps related to the SiF_6 vibrational modes discussed by Ihringer (1980). Consequently, all 002 reflections were eliminated from further processing. Other reflections did not appear to be similarly affected.

A low R_{int} was not expected in view of the high scan speed, but its value may to some degree reflect the difficulty of maintaining a stable crystal temperature during the measurements. Differential thermal expansion of the crystal arising from temperature fluctuations might also contribute to the intensity variation.

Five structural parameters together with a scale factor were refined by least-squares methods using neutral atom scattering factors (Cromer & Waber, 1974), including dispersion correction (Cromer, 1974). All calculations used the *Xtal*3.2 system of crystallographic programs (Olthof-Hazekamp, 1992). Least-squares refinement of a Zachariasen (1967) extinction parameter together with the structural parameters resulted in a minimum extinction factor of y_{min} = 1.0. That is, extinction was not significant. The refined positional and vibrational parameters were: $x(F)$ = 0.2095 (2), $U_{11}(K)$ = 0.0092 (2), U_{11}(Si) = 0.0064 (4), $U_{11}(F)$ = 0.0059 (8), $U_{22}(F)$ = 0.0140 (6) Å^2, where U_{ij} is defined by the equation $T(\mathbf{h}) = \exp(-2\pi^2\Sigma U_{ij}h_ih_jb_ib_j)$.

Relationships between the room-temperature vibrational parameters (Hester *et al.*, 1993*a*) persist at low temperature. The variable $x(F)$ positional parameter is larger at low temperature, because of the resistance of the Si—F bond length to contraction.

Reliability of deformation densities

The reliability of the $\Delta\rho$ maps obtained by Fourier transformation from F_o–F_c values must be assessed before firm conclusions are drawn. There are alternative approaches to this assessment. At points away from atomic centres and symmetry elements, an approximate measure of $\Delta\rho$ accuracy is provided by the $\sigma(\Delta\rho)$ expression of Cruickshank (1949). Corresponding values are included in Table 1. The significance of a region, rather than a point in a $\Delta\rho$ map, can also be calculated (Maslen, 1988). Alternatively, the reliability of $\Delta\rho$ results can be directly assessed by repeating the experiment. In addition to replication, the consistency of $\Delta\rho$ maps both internally and with other known information also helps to assess accuracy.

Table 2. *Low-temperature* K_2SiF_6 *data collection parameters* (002 *reflection excluded*)

Diffractometer	Syntex $P2_1$
Monochromator	Graphite (002)
a (Å)	8.046 (2)
Scan type	$\omega/2\theta$
Scan width (°)	$2.40 + 0.43\tan\theta$
Maximum $\sin\theta/\lambda$ (Å^{-1})	0.95
Number of reflections measured	5839
Instability factor	9.6×10^{-4}
μ (mm^{-1})	2.09
Transmission range	0.7980–0.8381
R_{int} (all reflections, I)*	0.1589
Number of independent reflections ($\lvert F_{hkl}\rvert \geq 0$)	129
R	0.070
Weighting scheme	$w = 1/\sigma^2(F)$
$wR = [(\Sigma w\lvert F_o - F_c\rvert^2)/\Sigma wF_o^2]^{1/2}$	0.024
S	1.47 (9)
y_{min}	1.0
Min., max. $\Delta\rho$ (e Å^{-3})	−1.8, 3.1

* For 1491 reflections with $I > 3\sigma(I)$, $R_{int} = 0.0625$.

The low $\sigma(\Delta\rho)$ values for the synchrotron radiation and the K_2NiF_4 experiments suggest that $\Delta\rho$ maps should be reliable. Repeating the K_2PdCl_4 low-temperature experiment confirmed the existence of $\Delta\rho$ features discussed in this paper. The reliability of the low-temperature K_2SiF_6 data is more difficult to assess. The rather large R_{int} for this data set, due to the high proportion of statistically inaccurate weak reflections, suggests that the reliability of conclusions drawn from these data could be limited. However, measurement of a full sphere for this cubic structure ensures that the number of equivalents for each reflection is large. The variances in F values determined for each independent reflection by averaging are not excessive. The commonly invoked global measures of data set accuracy, wR, S and $\sigma(\Delta\rho)$, do not indicate that this experiment should be uninformative. As the K_2SiF_6 low-temperature $\Delta\rho$ maps merit examination, the consistency of these maps with other information is discussed below.

Atomic charges

Atomic charges calculated by projecting the electron-difference density onto atomic-density basis functions (Hirshfeld, 1977) are listed in Table 3. Values for the low-temperature study of K_2SiF_6 are not presented because the 002 reflection was omitted. Because atomic charges are sensitive to low-order structure factors, omission could alter the values determined for that structure significantly.

Table 3. *Charges in |e| determined by Hirshfeld partitioning of* $\Delta\rho$

Compound	K	*M*	*X*1	*X*2
K_2SiF_6	−0.5 (1)	−0.01 (2)	+0.02 (1)	
K_2PdCl_6	−0.03 (4)	+2.23 (5)	−0.36 (5)	
K_2PdCl_4	−1.16 (9)	+2.8 (1)	−0.1 (1)	
K_2PdCl_4 (low temperature)	−0.4 (4)	+0.1	+0.2 (1)	
K_2NiF_4	+0.62 (2)	+0.35 (2)	−0.91 (2)	+0.12 (2)

The charges derived for different compounds show a limited degree of correspondence. The metal atom is either neutral or positive. Halide-atom charges tend to be negative. The K atoms, although having formal charges of +1, tend to acquire negative charges. There is a consistent trend for electrons to accumulate preferentially on the atoms indicated by the vibration amplitudes to be packed less tightly in the structure.

Interatomic electron densities

The accumulations and depletions of electron density in interatomic regions both for K_2PdCl_4 and K_2PdCl_6 at room temperature (Figs. 1 and 2) are significant. The K_2PdCl_4 $\Delta\rho$ maps are depleted in interatomic regions at $\frac{1}{2}$,0,0 (intersection of lines in Fig. 1*a*), at 0,0,$\frac{1}{2}$ (top left of Fig. 1*b*) and along the extension of the Pd—Cl bond at $\frac{1}{2}$,$\frac{1}{2}$,0. There is an oddly shaped depletion between the two K atoms at $\frac{1}{4}$, $\frac{1}{4}$, $\frac{1}{2}$ and significant accumulation near $\frac{1}{2}$, $\frac{1}{2}$, $\frac{1}{2}$. The fourfold symmetry about that point generates the regular feature at the bottom right of Fig. 1(*b*).

For K_2PdCl_6, there is strong depletion at 0,0,$\frac{1}{2}$ at the top left corner of Fig. 2, at $\frac{1}{4}$, $\frac{1}{4}$, $\frac{1}{2}$ and at $\frac{1}{4}$, $\frac{1}{4}$,0. The circular shapes of most K_2PdCl_6 depletions provide little evidence that differentiates real electron redistribution from experimental artefacts, in contrast with the anisotropically shaped K_2PdCl_4 depletions that relate closely to structural geometry. The lines connecting Cl atoms in neighbouring moieties in Fig. 1(*a*) do not overlap at right angles. The depletion centred at the intersection of these lines stretches along the Cl–Cl vectors, as is also true of the depletion along the extension of the Pd—Cl bond in the same figure.

The depletion at the centre of Fig 1(*b*) has a particularly obvious relationship to the K and Cl dispositions in this structure. There are Cl atoms, with fractional coordinates 0.23,0.23,0, located above and below this depletion, that also lie near the midpoint of the K atoms at 0,$\frac{1}{2}$, $\frac{1}{2}$ and $\frac{1}{2}$,0,$\frac{1}{2}$. The anisotropic shape of this depletion is aptly described by a superposition of an ovular depletion centred at the K—K midpoint $\frac{1}{4}$, $\frac{1}{4}$, $\frac{1}{2}$ and an ovular depletion centred at the Cl—Cl midpoint 0.23,0.23,$\frac{1}{2}$.

The obvious relationship of the structure in all these $\Delta\rho$ depletions to non-bonding interatomic contacts suggests that the depletion may be an effect of non-bonded interactions on the electron density. Depletion may arise because the fermionic nature of electrons forces the total wavefunction of an electronic system to be antisymmetric (Shankar, 1985). Thus, if electrons from two interacting atoms are spin-paired (antisymmetric spin component), the exchange contribution to the total energy is reduced by orbital overlap and a positive contribution to $\Delta\rho$ results. Conversely, if the electron spin component is symmetric, electrons are removed from the internuclear region. In the following, the term 'exchange' is used to indicate movement of electrons in order to satisfy the requirements for antisymmetrizing the total wavefunction. 'Exchange' effects implicitly

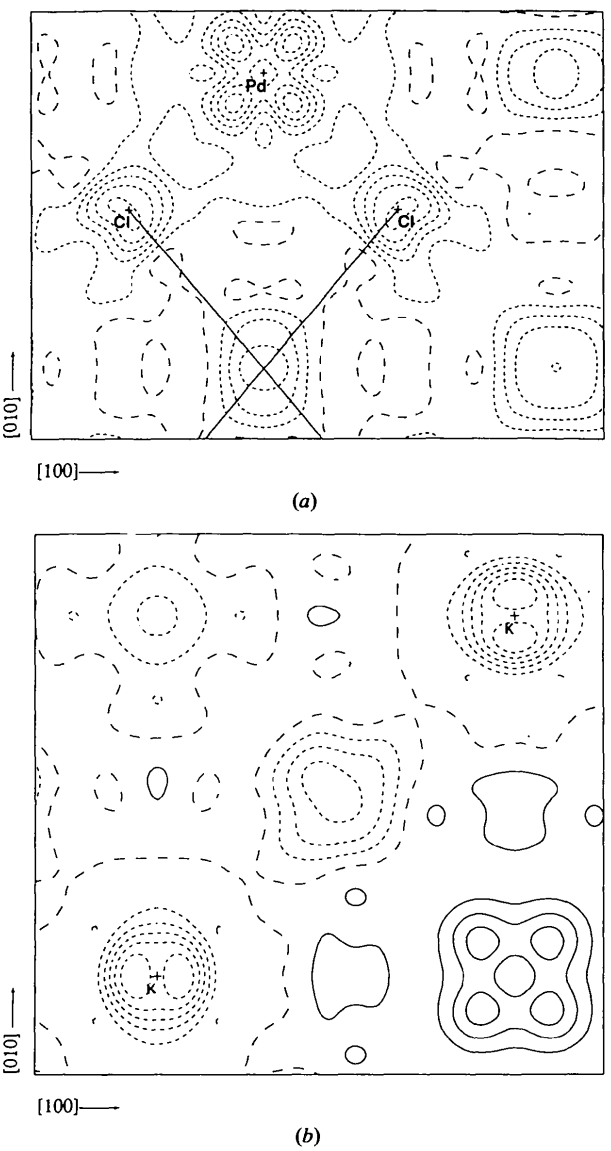

Fig. 1. $\Delta\rho$ in (*a*) z = 0 and (*b*) z = 1/2 planes for K_2PdCl_4. Borders: (*a*) 6.9 x 5.1 and (*b*) 5.6 x 5.3 Å; contour interval 0.2 e Å^{-3}. Positive contours solid, negative contours dashed, zero contour dot-dashed.

refer to electron-depleting exchange. The $\Delta\rho$ topography in perovskite-related structures has been attributed to exchange effects by Maslen & Spadaccini (1989).

Significant exchange depletion is expected if neighbouring closed-shell atoms overlap strongly. Depletion due to overlap for electrons with symmetric spin components should outweigh the concentration due to overlap for electrons with paired (antisymmetric) spin components in closed-shell systems. That explains electron-depleting overlap between Cl and K atoms. In K_2PdCl_6 such depletions occur at $0,0,\frac{1}{2}$ (upper left of Fig. 2) and $\frac{1}{4},\frac{1}{4},\frac{1}{2}$ (upper right of Fig. 2).

In tightly packed structures, electron-depleting exchange interactions naturally move electron density towards areas of the structure where electrons overlap less strongly. Electrons accumulate in the vicinity of the least tightly packed structural cavity at $\frac{1}{2},\frac{1}{2},\frac{1}{2}$ for K_2PdCl_4. The maximum accumulation is displaced slightly from the centre of the cavity, which appears to arise from weaker exchange depletion due to overlap of the four surrounding K atoms at $0,\frac{1}{2},\frac{1}{2}$, $\frac{1}{2},0,\frac{1}{2}$, $1,\frac{1}{2},\frac{1}{2}$ and $\frac{1}{2},1,\frac{1}{2}$. An approximately square depletion at $\frac{1}{2},\frac{1}{2},0$ (bottom right in Fig. 1*a*) results when a structural cavity is surrounded by four equidistant Cl atoms arranged in a square. Superimposition of a square depletion on a broad accumulation of electrons would account for the $\Delta\rho$ topography at $\frac{1}{2},\frac{1}{2},\frac{1}{2}$. Electron transfer by exchange provides a simple, self-consistent explanation for all significant features in the interatomic regions for these maps.

To check the hypothesis that electron exchange affects the $\Delta\rho$ topography in structural cavities significantly, data from the recent experiment on K_2NiF_4 by Yeh *et al.* (1993) were used to generate $\Delta\rho$ maps, using the extinction parameter determined as part of a least-squares structure refinement. To minimize correlation of the scale factor with the extinction parameter, the scale and vibrational parameters were refined using high-order data ($\sin\theta/\lambda > 0.6$) before refining the Zachariasen (1967) secondary extinction parameter with the whole data set.

The vibrational and positional parameters were similar to those reported by Yeh *et al.* (1993) for their high-angle refinement. The $\Delta\rho$ map for the $z = 0$ plane agrees closely with that for the $z = 0$ plane of the cubic perovskite $KNiF_3$ (Maslen & Spadaccini, 1989) where the disposition of atoms is similar, in having low positive density around the F1 atom, and similar $\Delta\rho$ topography both near the Ni atom and along the vector from Ni to the structural cavity. The electron density at the structural cavity in the centre of the K_2NiF_4 base plane is depleted less strongly than that in $KNiF_3$.

A $\Delta\rho$ map for the (100) plane containing K–F halide vectors, presented in Fig. 3, includes all symmetry-independent structural cavities. The density is depleted at the structural cavities at $0,0,\frac{1}{2}$, $0,\frac{1}{2},z$(F2) and at $0,\frac{1}{2},z$(K). There is no depletion at the centre of the cavity bordered by K, F2, Ni and F1 (left of bottom centre in Fig. 3) supporting the hypothesis that depletion occurs mainly at the midpoints of interatomic contacts between similar species. The centre of the cavity is at the midpoint of a 6.5 Å long F1–F1 vector, but no other interatomic vector midpoints are located there. By analogy with the K_2SiF_6 maps, little depletion is expected along such long F–F vectors. The three large depletions in Fig. 3 are at the midpoints of the K–K contacts. The largest, at the top left corner, corresponds to the structural cavity depletion in $KNiF_3$. It is presumably more pronounced because of closer packing in the immediate environment.

Correlation of $\Delta\rho$ topography with structure is so strong that these topographical features are unlikely to originate in data processing artefacts. A physical explanation relating the $\Delta\rho$ features to the geometrical arrangement of the atoms in the structure is indicated.

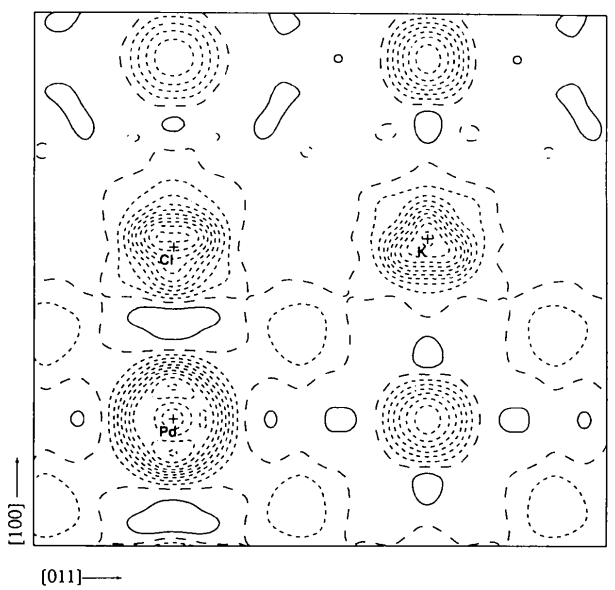

Fig. 2. $\Delta\rho$ in the (110) plane for K_2PdCl_6; borders 7.7 x 7.1 Å, contours as in Fig 1.

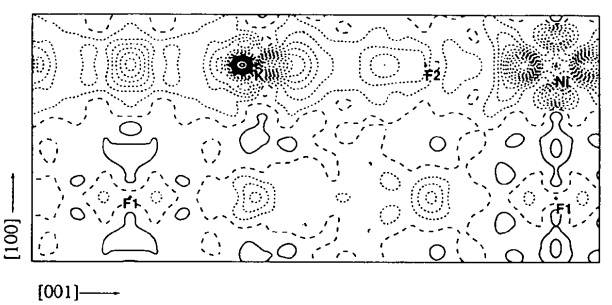

Fig. 3. $\Delta\rho$ in the (100) plane of K_2NiF_4; borders 8.7 x 3.7 Å, contour interval 0.2 e Å^{-3}.

The essential problem is to explain how depletion of the order 1 e Å^{-3} occurs in regions of the map where the promolecular contribution for atoms at rest is small.

It is difficult to understand why atoms separated by 7 Å should display what appears to be exchange interference in precise diffraction images. Nevertheless, other experiments support the present results. Large-scale fluctuations in electron states in two-dimensional cavities were observed in scanning tunnelling microscope images by Crommie, Lutz & Eigler (1993), who report marked increases in the local density of electron states at the centre of a ring of Fe atoms with a 71 Å radius. Their observations were justified on quantum mechanical grounds.

K-atom densities

There is structure in the $\Delta\rho$ maps near the K-atom nuclei for all three compounds. The features for the isomorphic compounds K_2PdCl_6 and K_2SiF_6 are topographically similar. In both cases electron depletion along the K–Pd vector is stronger than that along a vector at right angles. The features around the K atom for the isomorphic K_2PtCl_6 compound in corresponding $\Delta\rho$ maps obtained by Restori & Schwarzenbach (1993) closely resemble those around K in K_2SiF_6, shown in Fig 4. The heights of the difference-density peaks for the K_2PdCl_6 and K_2SiF_6 structures differ, perhaps because the approach to extinction correction differs in the two studies. When a least-squares extinction correction similar to that used by Restori & Schwarzenbach (1993) is applied to the K_2PdCl_6 data of Hester *et al.* (1993*a*), positive features similar to those observed for the other compounds appear. A change in the scale factor affects the strong low-angle reflections significantly, but in so far as the local topography is derived from the bulk of the reflections which, being weaker, are affected less strongly by the scale factor, the topographies correspond closely.

The possibility that anharmonic atomic vibration explains these features must be considered, especially as Restori & Schwarzenbach (1993) refined anharmonic vibration parameters for the K atom, rendering $\Delta\rho$ in that vicinity essentially flat. That is consistent with the hypothesis that the sharper $\Delta\rho$ features near the K nuclei are due to anharmonicity, but does not eliminate electron redistribution as an alternative. As pointed out by Buttner & Maslen (1992), $\Delta\rho$ features due to anharmonicity may closely resemble those due to bonding electron redistribution. Because it is difficult to differentiate between the alternative hypotheses in a single experiment *a priori*, one must invoke other evidence.

Whereas $\Delta\rho$ due to anharmonicity should increase with temperature, electron redistribution due to bonding is more prominent at low temperature, because of reduced vibrational smearing of the difference density. A low-temperature X-ray diffraction experiment should contain evidence that distinguishes between anharmonic and electronic origins for $\Delta\rho$ features. Although the low-temperature experiment on K_2SiF_6 described above is not particularly accurate, $\Delta\rho$ features due to bonding have higher significance if the atomic numbers for all the atoms in a compound are low. In the relevant low-temperature $\Delta\rho$ section depicted in Fig. 4(*b*), the contour interval is four times that for the room-temperature map shown in Fig. 4(*a*).

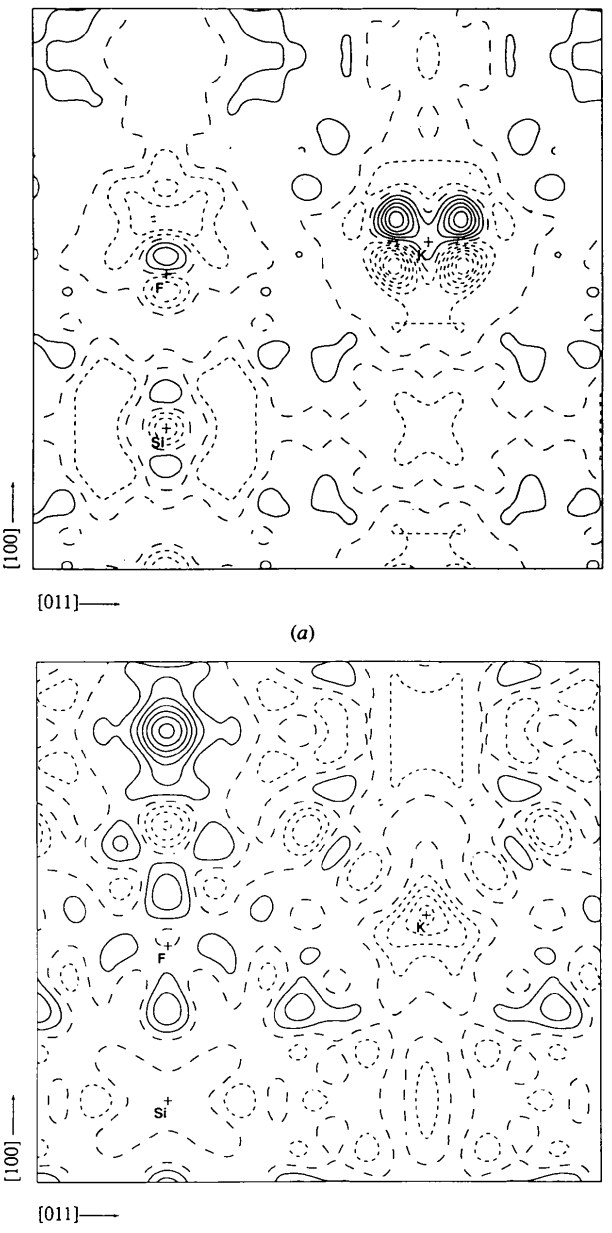

Fig. 4. $\Delta\rho$ in the K_2SiF_6 (110) plane. (*a*) Room temperature, contour interval 0.1 e Å^{-3}, and (*b*) low temperature, contour interval 0.4 e Å^{-3}. Borders 6.2 x 5.7 Å.

and mounted in a steady stream of boil-off nitrogen on a $P2_1$ diffractometer. A temperature of 110 (10) K was maintained by monitoring thermocouple measurements at the exit nozzle, adjusting the current through a small heater in the gas stream automatically.

Two complete spheres of data were measured at a constant scan rate of 12° min^{-1}. The high scan rate minimized condensation of ice that tended to form if the goniometer head was stationary for long periods. Experimental details are listed in Table 2.

All 002 reflections and equivalents, measured twice for a total of 12 measurements, had atypical profiles that were either flat or sloped upwards in a positive $\omega/2\theta$ direction. The weak reflections with strongly sloping profiles had unusually imbalanced backgrounds, leading in several cases to net negative intensities. These uneven backgrounds appear to be connected to strong, asymmetric diffuse scattering, perhaps related to the SiF_6 vibrational modes discussed by Ihringer (1980). Consequently, all 002 reflections were eliminated from further processing. Other reflections did not appear to be similarly affected.

A low R_{int} was not expected in view of the high scan speed, but its value may to some degree reflect the difficulty of maintaining a stable crystal temperature during the measurements. Differential thermal expansion of the crystal arising from temperature fluctuations might also contribute to the intensity variation.

Five structural parameters together with a scale factor were refined by least-squares methods using neutral atom scattering factors (Cromer & Waber, 1974), including dispersion correction (Cromer, 1974). All calculations used the *Xtal*3.2 system of crystallographic programs (Olthof-Hazekamp, 1992). Least-squares refinement of a Zachariasen (1967) extinction parameter together with the structural parameters resulted in a minimum extinction factor of y_{min} = 1.0. That is, extinction was not significant. The refined positional and vibrational parameters were: $x(F)$ = 0.2095 (2), $U_{11}(K)$ = 0.0092 (2), U_{11}(Si) = 0.0064 (4), $U_{11}(F)$ = 0.0059 (8), $U_{22}(F)$ = 0.0140 (6) Å^2, where U_{ij} is defined by the equation $T(\mathbf{h}) = \exp(-2\pi^2\Sigma U_{ij}h_ih_jb_ib_j)$.

Relationships between the room-temperature vibrational parameters (Hester *et al.*, 1993*a*) persist at low temperature. The variable $x(F)$ positional parameter is larger at low temperature, because of the resistance of the Si—F bond length to contraction.

Reliability of deformation densities

The reliability of the $\Delta\rho$ maps obtained by Fourier transformation from F_o–F_c values must be assessed before firm conclusions are drawn. There are alternative approaches to this assessment. At points away from atomic centres and symmetry elements, an approximate measure of $\Delta\rho$ accuracy is provided by the $\sigma(\Delta\rho)$ expression of Cruickshank (1949). Corresponding values are included in Table 1. The significance of a region, rather than a point in a $\Delta\rho$ map, can also be calculated (Maslen, 1988). Alternatively, the reliability of $\Delta\rho$ results can be directly assessed by repeating the experiment. In addition to replication, the consistency of $\Delta\rho$ maps both internally and with other known information also helps to assess accuracy.

Table 2. *Low-temperature* K_2SiF_6 *data collection parameters* (002 *reflection excluded*)

Diffractometer	Syntex $P2_1$
Monochromator	Graphite (002)
a (Å)	8.046 (2)
Scan type	$\omega/2\theta$
Scan width (°)	$2.40 + 0.43 \tan\theta$
Maximum $\sin\theta/\lambda$ (Å^{-1})	0.95
Number of reflections measured	5839
Instability factor	9.6×10^{-4}
μ (mm^{-1})	2.09
Transmission range	0.7980–0.8381
R_{int} (all reflections, I)*	0.1589
Number of independent reflections ($\|F_{hkl}\| \geq 0$)	129
R	0.070
Weighting scheme	$w = 1/\sigma^2(F)$
$wR = [(\Sigma w\|F_o - F_c\|^2)/\Sigma wF_o^2]^{1/2}$	0.024
S	1.47 (9)
y_{min}	1.0
Min., max. $\Delta\rho$ (e Å^{-3})	−1.8, 3.1

* For 1491 reflections with $I > 3\sigma(I)$, R_{int} = 0.0625.

The low $\sigma(\Delta\rho)$ values for the synchrotron radiation and the K_2NiF_4 experiments suggest that $\Delta\rho$ maps should be reliable. Repeating the K_2PdCl_4 low-temperature experiment confirmed the existence of $\Delta\rho$ features discussed in this paper. The reliability of the low-temperature K_2SiF_6 data is more difficult to assess. The rather large R_{int} for this data set, due to the high proportion of statistically inaccurate weak reflections, suggests that the reliability of conclusions drawn from these data could be limited. However, measurement of a full sphere for this cubic structure ensures that the number of equivalents for each reflection is large. The variances in F values determined for each independent reflection by averaging are not excessive. The commonly invoked global measures of data set accuracy, wR, S and $\sigma(\Delta\rho)$, do not indicate that this experiment should be uninformative. As the K_2SiF_6 low-temperature $\Delta\rho$ maps merit examination, the consistency of these maps with other information is discussed below.

Atomic charges

Atomic charges calculated by projecting the electron-difference density onto atomic-density basis functions (Hirshfeld, 1977) are listed in Table 3. Values for the low-temperature study of K_2SiF_6 are not presented because the 002 reflection was omitted. Because atomic charges are sensitive to low-order structure factors, omission could alter the values determined for that structure significantly.

in Fig. 5(*b*) is based on the deposited data of Takazawa *et al.* (1988), with which our new experiment is consistent.

The room-temperature $\Delta\rho$ map shown in Fig. 4(*a*) contains a boomerang-shaped hollow around the Cl atom, consistent with libration of the Cl atom within a rigid $PdCl_4$ moiety. The density on the Pd side of the Cl atom is more negative than that immediately behind the Cl atom. The pronounced change in the low-temperature difference-density topography is fully consistent with reduced librational motion for the Cl atom. This change in $\Delta\rho$ topography around the Cl atom in K_2PdCl_4 reinforces the conclusions from the study of the F atoms in K_2SiF_6.

The K-atom difference density for K_2PdCl_4 is, in marked contrast to Cl, more prominent at low temperature, partly due to improved resolution. As the K-atom features are not reduced at low temperature, the hypothesis that these reflect bonding electron redistribution is reinforced. Taken in isolation the K_2SiF_6 room- and low-temperature experiments imply a need for caution before attributing K-atom $\Delta\rho$ features to the effect of anharmonic vibrations. In conjunction with the K_2PdCl_4 room- and low-temperature studies, they provide persuasive evidence for sharp deformation of the K-atom electron density when a crystal forms.

Strong librational motion of the F atom in K_2NiF_4 is not expected because the NiF_6 groups are connected at their corners. The $\Delta\rho$ topography near the K atom is complex. There is strong depletion along the K–F2 vector. Somewhat smaller depletions along the K–Ni vectors are analogous to those observed along the K–Si vector in K_2SiF_6. These depletions are oriented towards the vertices of a square pyramid centred around the K nucleus. A small but strong accumulation of electron density close to the nucleus is oriented toward the centre of the base of the pyramid, a direction that corresponds to the K–K contact through the centre of the structural cavity. Based on the results from the other compounds, it is reasonable to associate these features with bonding electron redistribution.

Possible explanations for features near K atoms in these structures are K–Pd interactions in K_2PdCl_4 and K–K interactions in the K_2SiF_6 series. Metal–metal bonds, associated with peaks around 1 Å from the nucleus, have been reported previously (Hester, Maslen, Glazer & Stadnicka, 1993). The dual-lobed structure in the $\Delta\rho$ sections for the K_2SiF_6 series of compounds is attributable to a well-defined three-dimensional disposition of K-atom depletion lobes. There is another pair of depletion lobes above the nucleus in a plane perpendicular to that presented here. A slight extension of these lobes into the plane presented here bisects what would otherwise be a more uniform electron accumulation.

The authors wish to thank Professor Yu Wang for kindly providing K_2NiF_4 structure factors. This work was supported by the Australian Research Council.

Addendum

A referee suggested that interatomic features discussed in this paper might arise from poorly determined scale factors. The scale factor was varied by 3σ for all the data sets discussed here. The electron density in interatomic regions was not affected significantly.

References

BUTTNER, R. H. & MASLEN, E. N. (1992). *Acta Cryst.* B**48**, 644–649.

BUTTNER, R. H., MASLEN, E. N. & SPADACCINI, N. (1990). *Acta Cryst.* B**46**, 131–138.

CROMER, D. T. (1974). *International Tables for X-ray Crystallography*, Vol. IV, pp. 148–150. Birmingham: Kynoch Press. (Present distributor Kluwer Academic Publishers, Dordrecht.)

CROMER, D. T. & WABER, J. T. (1974). *International Tables for X-ray Crystallography*, Vol. IV, pp. 71–147. Birmingham: Kynoch Press. (Present distributor: Kluwer Academic Publishers, Dordrecht.)

CROMMIE, M. F., LUTZ, C. P. & EIGLER, D. M. (1993). *Science*, **262**, 218–220.

CRUICKSHANK, D. W. J. (1949). *Acta Cryst.* **2**, 65–82.

HESTER, J. R., MASLEN, E. N., GLAZER, M. & STADNICKA, K. (1993). *Acta Cryst.* B**49**, 641–646.

HESTER, J. R., MASLEN, E. N., SPADACCINI, N., ISHIZAWA, N. & SATOW, Y. (1993*a*). *Acta Cryst.* B**49**, 967–973.

HESTER, J. R., MASLEN, E. N., SPADACCINI, N., ISHIZAWA, N. & SATOW, Y. (1993*b*). *Acta Cryst.* B**49**, 842–846.

HIRSHFELD, F. L. (1977). *Isr. J. Chem.* **16**, 198–201.

IHRINGER, J. (1980). *Acta Cryst.* A**36**, 89–96.

KIJIMA, N., TANAKA, K. & MARUMO, F. (1983). *Acta Cryst.* B**39**, 557–561.

MASLEN, E. N. (1988). *Acta Cryst.* A**44**, 33–37.

MASLEN, E. N. & SPADACCINI, N. (1989). *Acta Cryst.* B**45**, 45–52.

MASLEN, E. N., SPADACCINI, N., ITO, T., MARUMO, F., TANAKA, K. & SATOW, Y. (1993). *Acta Cryst.* B**49**, 632–636.

OLTHOF-HAZEKAMP, R. (1992). *CRYLSQ*. In *Xtal*3.2 *Reference Manual*, edited by S. R. HALL, H. D. FLACK & J. M. STEWART. Univs. of Western Australia, Australia, Geneva, Switzerland, and Maryland, USA.

RESTORI, R. & SCHWARZENBACH, D. (1993). *Z. Naturforsch.* **48**, 12–20.

SHANKAR, R. (1985). *Principles of Quantum Mechanics*, Ch. 10. New York: Plenum Press.

TAKAZAWA, H., OHBA, S. & SAITO, Y. (1988). *Acta Cryst.* B**44**, 580–585.

YEH, S. K., WU, S. Y., LEE, C. S. & WANG, Y. (1993). *Acta Cryst.* B**49**, 806–811.

ZACHARIASEN, W. H. (1967). *Acta Cryst.* **23**, 558–564.